Terahertz Second-Harmonic Generation from Lightwave Acceleration of Symmetry-Breaking Nonlinear Supercurrents

C. Vaswani,[1,*] M. Mootz,[2,*] C. Sundahl,[3,*] D. H. Mudiyanselage,[1] J. H. Kang,[3] X. Yang,[1] D. Cheng,[1] C. Huang,[1] R. H. J. Kim,[1] Z. Liu,[1] L. Luo,[1] I. E. Perakis,[2] C. B. Eom,[3] and J. Wang[1,†]

[1]*Department of Physics and Astronomy and Ames Laboratory-U.S. DOE, Iowa State University, Ames, Iowa 50011, USA*
[2]*Department of Physics, University of Alabama at Birmingham, Birmingham, Alabama 35294-1170, USA*
[3]*Department of Materials Science and Engineering, University of Wisconsin-Madison, Madison, Wisconsin 53706, USA*

We report terahertz (THz) light-induced second harmonic generation, in superconductors with inversion symmetry that forbid even-order nonlinearities. The THz second harmonic emission vanishes above the superconductor critical temperature and arises from precession of twisted Anderson pseudospins at a multicycle, THz driving frequency that is not allowed by equilibrium symmetry. We explain the microscopic physics by a dynamical symmetry breaking principle at sub-THz-cycle by using quantum kinetic modeling of the interplay between strong THz-lightwave nonlinearity and pulse propagation. The resulting nonzero integrated pulse area inside the superconductor leads to light-induced nonlinear supercurrents due to subcycle Cooper pair acceleration, in contrast to dc-biased superconductors, which can be controlled by the band structure and THz driving field below the superconducting gap.

The determination and understanding of symmetry breaking in superconducting states has been a central theme in condensed matter physics that remains challenging. A recent example is second harmonic generation (SHG) at optical frequencies that is actively explored in cuprates and other inversion-symmetry-breaking superconductors [1]. Such studies reveal that, in addition to the underlying crystal structure, the quantum order itself can also lead to nontrivial SHG signals. In contrast to high energy optical excitation, the advent of intense few- and multi-cycle THz pulses has opened new opportunities for exploring fundamental nonlinear physics and broken symmetry states [2]. Multicycle phase-locked THz pulses tuned below the pair-breaking energy gap $2\Delta_{SC}$ minimally perturb superconductor (SC) states. In contrast, optical pumping tends to destroy SC order by heating the quasiparticles (QPs) [3]. In addition, while the carrier-envelope phase-unlocked pulses used for optical pumping are sensitive to SHG, they are not suitable for identifying subcycle lightwave modulation effects that relate to the oscillating pump E field. THz-induced nonlinear effects in SCs have been of interest lately, e.g., collective modes [4–10], stripe phases [11], gapless quantum fluid with minimal scattering [12], and high harmonics in coherent pump-probe responses [13]. However, THz SHG (T-SHG) from single-pulse excitation of SCs, a fundamentally new quantum phenomena, has not been observed so far until this work.

SHG may be observed in SCs with an additional inversion symmetry breaking order parameter coming, e.g., from pseudogap, magnetic, charge, or lattice coupled orders. However, the *spontaneous* coherence between Cooper pairs ($\mathbf{k}\uparrow$, $-\mathbf{k}\downarrow$) in a simple BCS ground state does not support SHG, due to the inversion symmetry. Nevertheless, *driven* coherence by strong acceleration of macroscopic Cooper pair center-of-mass (CM) motion can transiently break the equilibrium inversion symmetry without pair breaking, via a periodically modulated superfluid momentum, $\mathbf{p}_s(t) \propto \int_{-\infty}^{t} d\tau \mathbf{E}_{eff}(\tau)$. Such time-dependent preferred direction can be introduced by phase-locked THz electric field pulses tuned below the $2\Delta_{SC}$ gap, which induce an effective local electric field $\mathbf{E}_{eff}(\tau)$ determined by the electromagnetic fields and by spatial gradients of the chemical potential and scalar fields. Figure 1(a) illustrates the quantum dynamics of the BCS state driven by an ac field, arising from precession of "twisted" Anderson pseudospins (PSs) mapped onto the Bloch sphere. In such picture, the PSs respond to a pseudomagnetic field controlled by THz driving, whose x and y components (transverse) are given by the complex SC order parameter, whereas its z component (longitudinal) is determined by the band structure. Cooper pair "lightwave" acceleration can nonadiabatically drive a *supercurrent–carrying* transient macroscopic state, with oscillating condensate momentum $\mathbf{p}_s(t)$ [black arrow, Fig. 1(a)], consisting of pairs $[\mathbf{k} + \mathbf{p}_s(t)\uparrow, -\mathbf{k} + \mathbf{p}_s(t)\downarrow]$ [13]. The resulting nonlinear supercurrent flow breaks the equilibrium symmetry that gives rise to symmetry-breaking PS dynamics. Such PS oscillations have manifested themselves in the forbidden third-harmonic peaks observed in the two-pulse pump-probe spectra of sufficiently clean Nb_3Sn SCs [13]. However, single-pulse T-SHG emission, a hallmark for
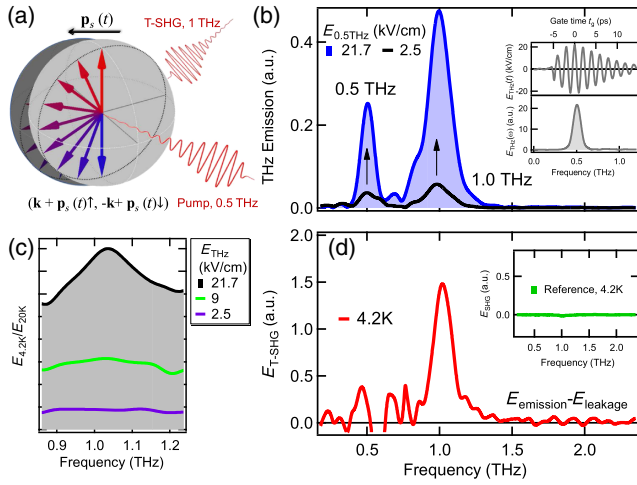
FIG. 1. (a) SHG by THz lightwave acceleration of superfluid momentum, $\mathbf{p}_s(t)$. (b) THz emission for two E-field strengths, 21.7 kV/cm (blue) and 2.5 kV/cm (black). Inset: 0.5 THz multicycle phase-locked THz pulse and spectrum. (c) THz emission at 4.2K normalized to the emission at 20K for various THz E-field strengths (traces offset for clarity). (d) The THz SHG contribution after subtracting the pump leakage (main text). Inset: SHG emission from the substrate.

the broken-symmetry state, and microscopic theory of asymmetric light pulses are still elusive, raising questions about the interpretation of the pump-probe signals in Ref. [13]. This lightwave current driving is also distinct from the dc-biased SCs from, e.g., applied electrodes [14]. Two outstanding questions remain for the microscopic physics: (i) how can an *asymmetric* ac electric field pulse with nonzero pulse area $\int_{-\infty}^{\infty} d\tau \mathbf{E}(\tau) \neq 0$, i.e., a zero-frequency (dc) component, be generated in SCs? (ii) what are the band structure effects, where flat bands close to the Fermi level result in a large density of states (DOS), on the light-induced supercurrent?

In this Letter, we provide first evidence of single-pulse THz SHG emission exclusively in the SC state of Nb_3Sn. Our nonlinear quantum kinetic calculations, based on gauge invariant density matrix equations of motion, describe a microscopic mechanism for photogenerating a broken symmetry nonlinear supercurrent with low-frequency components in the forward- and backward-traveling THz electric fields in the presence of PS nonlinearity, controlled by the band structure and THz field.

Our sample consists of a 20 nm thick Nb_3Sn film grown by magnetron sputtering on an Al_2O_3 substrate. $T_c \sim 16$ K and SC gap $2\Delta_{SC} \sim 4.5$ meV [3,15]. 2 W, 35 fs pulses from a Ti:sapphire-based regenerative amplifier were used to generate broadband quasi-single-cycle THz pulses from a $LiNbO_3$ crystal, via a tilted-pulse-front scheme [12,16,17]. The peak multicycle electric field, $E_{0.5\ THz} \sim 20$ kV cm^{-1}, at 2.1 meV (0.5 THz) is shown in the inset of Fig. 1(b) along with the pulse spectrum. For the results presented below, a 4.2 meV (1.0 THz) narrow band pass filter was

placed after the sample to block the fundamental beam and extract the nonlinear emission signal [18].

Figures 1(b)–1(c) show the observation of T-SHG emission at 1.0 THz for various field strengths $E_{0.5\ THz}$. These THz emission signals are, however, a mixture of both linear (THz pump background) and nonlinear responses, since it is not possible to completely filter out the pump. This is evident in Fig. 1(b), which plots the THz emission from our sample for THz pump E-field strengths of $E_{0.5\ THz} = 21.7$ kV/cm and 2.5 kV/cm. A signal at 0.5 THz is clearly visible even after the 1.0 THz filter is placed after the sample, due to residual leakage of 0.5 THz radiation through the 1.0 THz filter. Likewise, a portion of the signal at 1.0 THz should arise from leakage of 1.0 THz radiation from the 0.5 THz filter placed in the pump's path before the excitation to narrow the broadband THz pump spectrum. To extract the nonlinear contribution to the T-SHG emission coming from the SC order, Fig. 1(c) shows the ∼1.0 THz signals at 4.2 K normalized to the normal state value measured at 20 K, i.e., $E_{4.2K}/E_{20K}$, for various field strengths $E_{0.5\ THz} = 21.7, 9, 2.5$ kV cm^{-1}. For high E fields (black and green lines), the emission at 1.0 THz shows a clear resonance with temperature dependence, which diminishes at low E fields. In contrast, the 2.5 kV/cm trace (purple line) shows a flat, temperature-independent SHG signal, attributed to pump leakage. For the $E_{max} = 21.7$ kV cm^{-1} trace, the nonlinear contribution becomes dominant over the pump leakage, which underpins a dynamically generated T-SHG effect. We can quantitatively determine SHG field conversion efficiency as 3×10^{-3} with an estimated, very large nonlinear coefficient $\chi_{eff}^{(2)} \sim 1.27 \times 10^{-5}$ m/V, i.e., nearly three orders of magnitude larger than that of $LaTiO_3$ (see the Supplemental Material [19]).

To further corroborate the second order nature of the nonlinear THz emission in Fig. 1(c), we subtract the pump leakage contribution to the measured THz transmission with the following procedure. The pump leakage contribution for a given E-field strength can be obtained by scaling the low field data at 2.5 kV/cm according to the leakage ratio obtained from the THz polarizer angle. The results are shown in Fig. 1(d) for 21.7 kV/cm at 4.2 K, which shows a well-defined resonance at $2\omega_{THz}$. Note also there is no measurable T-SHG signal from the sapphire substrate [inset, Fig. 1(d)]. Figure 2(a) shows the E-field dependence of the T-SHG signal extracted from the measured emission as above. The peak of this T-SHG contribution is plotted against the square of the normalized E-field strength $(E_{THz}/E_{max})^2$ in Fig. 2(b). The observed E dependence is well reproduced by a linear fit, as expected for a second-order nonlinear optical process, i.e., proportional to E_{THz}^2. Note that any residual contribution from filter leakage should be linear in E_{THz}. Moreover, the second order behavior indicates the T-SHG effect is still in the perturbative regime, which is consistent with fact that
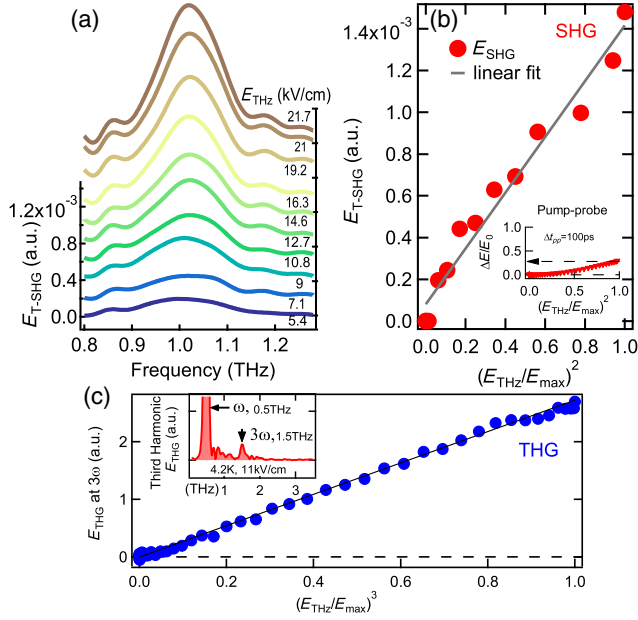
FIG. 2. (a) THz SHG signals for various E-field strengths at 4.2 K (traces offset for clarity). (b) THz SHG at 1 THz as function of the E-field strength normalized by E_{max} used. The grey line shows a linear fit to the data. Inset: THz pump-THz probe differential transmission $\Delta E/E_0$ as a function of THz driving field $(E_{THz}/E_{max})^2$ for time delay $\Delta t_{pp} = 100$ ps (maximum signal size) shows weak quench of SC state marked by a dash line. (c) THz third harmonic generation THG at 1.5 THz as function of the cube .of the E-field strength normalized by E_{max} used. Inset: THz emission for field strength 11 kV/cm showing the THG signal.

FIG. 3. (a) THz-SHG signals scaled to the E field transmittance at various temperatures normalized by the 20 K data (see text, traces offset for clarity). (b) Temperature dependence of the integrated spectral weight of THz SHG signals.

the THz pump–THz probe differential transmission $\Delta E/E_0$ as a function of THz driving [inset, Fig. 2(b)] shows a weak quench of SC coherence up to the E_{max} used. In addition, as shown in Fig. 2(c), this is also consistent with conventional third harmonic emission signals at 1.5 THz (inset) proportional to E_{pump}^3.

Figure 3(a) shows the strong temperature dependence of the above T-SHG emission. To accurately extract this SHG temperature dependence, we must account for the change in THz transmission due to temperature dependence of the E-field transmittance. This was done by normalizing the measured THz emission signals E_T/E_{20K}, Fig. 1(c), at each temperature T by the transmittance $(T = E_{Sample}/E_{Reference})$ at that temperature. The resulting quantity, $(E_T/T_T)/(E_{20K}/T_{20K})$, should describe the temperature dependence of the T-SHG contribution. This T-SHG resonance at $2\omega_{THz}$ vanishes, with a fairly consistent, resonant line shape, at the critical temperature $T_c \sim 16$ K, Fig. 3(b). The measured temperature dependence roughly follows that of the SC order parameter, which indicates that the origin of the forbidden T-SHG behavior is lightwave acceleration of nonlinear supercurrent, rather than some other contribution such as surface effect. Vanishing T-SHG in normal metallic
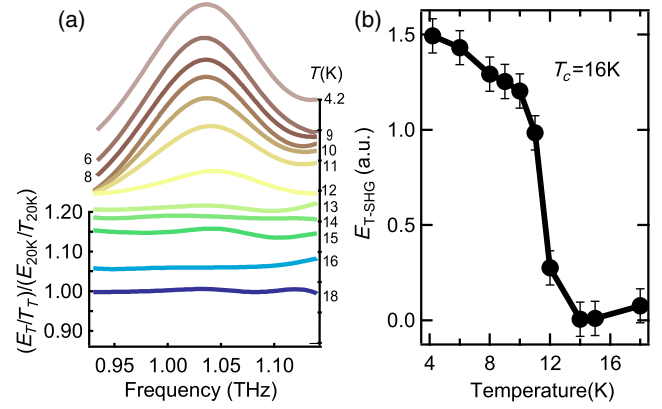
state can be understood as the absence of PS nonlinearities and stronger QP scattering.

To model our proposed mechanism for nonlinear light-wave supercurrent photogeneration, we extend previous studies of quantum transport [13,25,26] and third harmonic generation (THG) [27,28] in SCs by including the self-consistent interaction of the SC system with the propagating electromagnetic field (see the Supplemental Material [19]). The subcycle time dependence is described in a gauge-invariant way by generalizing the treatment of analogous ultrafast quantum kinetic transport effects in semiconductors to include the off-diagonal long range order [29]. We thus derive gauge-invariant SC Bloch equations [13] after subsequent gradient expansion of the spatial fluctuations [29]. Together with Maxwell's equations, we thus describe the dynamical interplay of three different THz-light-induced ultrafast effects: (1) light-wave nonlinear acceleration of the Cooper-pair condensate, (2) Anderson PS nonlinear precession, and (3) THz light-wave propagation inside the SC thin film. The latter propagation effects are required for photogeneration of a dc component in the presence of SC nonlinear response. The latter is due to both THz-light-induced condensate acceleration and PS precession which affects the interference between incident and reflected propagating waves.

Based on Maxwell's equations, any physical source of electromagnetic waves cannot contain a zero-frequency dc component [30]: $\int_{-\infty}^{\infty} dt E_{THz}(t) = 0$. However, this does not apply to reflected and transmitted electric field pulses after interaction with a nonlinear medium. A dynamical broken-symmetry dc supercurrent is photogenerated via the following steps. First, THz excitation of the SC with $E_{THz}(t)$ creates a nonlinear ac supercurrent $J(t)$, which then generates an electric field that interferes with the forward- and reflected backward-traveling THz electric fields inside the nonlinear SC. Such interference results in time-asymmetric reflected $[E_{ref}(t)]$ and transmitted

[$E_{\text{trans}}(t)$] electric field pulses with $\int_{-\infty}^{\infty} dt E_{\text{ref,trans}}(t) \neq 0$ inside the SC. The static component of the THz-light-induced current is the source of a zero-frequency component of the subpulses [30]. The strength of this photo-generated component of the reflected and transmitted electric fields depends on the THz-light-induced SC non-linearities. The latter are controlled by the effective local field spectral and temporal properties, as well as by the intensity of the applied pump E field and the band structure, discussed below. In the second step, the SC interaction with the above dynamically generated asymmetric effective electric field pulse breaks the equilibrium inversion symmetry and induces a Cooper-pair condensate flow. The latter can persist well after the pulse assuming weak photocurrent relaxation.

Figure 4(a) illustrates the calculated supercurrent photo-generation via THz pulse propagation inside the SC system. The external pump electric field $E_{\text{THz}}(t)$ (shaded area) is shown together with the photoinduced current $J(t)$ resulting from our calculation without (black line) and with propagation effects (red line). We used $E_{\text{THz}}(t) = \tilde{E}(t) \sin(\omega_{\text{pump}} t)$ with Gaussian envelope $\tilde{E}(t)$, which satisfies $\int_{-\infty}^{\infty} dt E_{\text{THz}}(t) = 0$. The pump frequency $\omega_{\text{pump}} = 2.1$ meV is well below the SC gap $2\Delta_{\text{SC}} = 4.5$ meV while the pulse duration ~ 20 ps is similar to the experimental pump pulse [inset Fig. 1(b)]. The photoinduced super-current resulting from our calculation including propaga-tion effects (red line) remains finite after the pulse, in contrast to the result without THz light wave propagation (black line). This demonstrates that a significant dc component of the photocurrent can be induced by THz lightwave propagation inside a SC thin film as discussed above. The calculated decay of this photoinduced dc supercurrent after the pulse here comes from radiative damping and results from self-consistent coupling between the current and laser field.

The predicted inversion-symmetry breaking in the non-equilibrium moving condensate is experimentally detect-able via high harmonics generation emitted at equilibrium-symmetry-forbidden frequencies. This is demonstrated in Figs. 4(c) and 4(e), where the spectra of the pump electric field and the currents of Fig. 4(a) are shown in linear and semilogarithmic scale, respectively. The spectrum of the current resulting from our calculation including THz light-wave propagation (red line) exhibits an equilibrium-sym-metry forbidden SHG (vertical dashed line), as well as a pronounced zero-frequency component. These contribu-tions are in addition to the equilibrium-symmetry-allowed linear and THG (vertical solid lines). In comparison, the spectrum of the current resulting from our calculation without THz–lightwave propagation effects (black line) shows only odd harmonics, as expected. We conclude that THz-light-induced nonlinearities, together with THz–light-wave propagation inside the SC system, can induce a
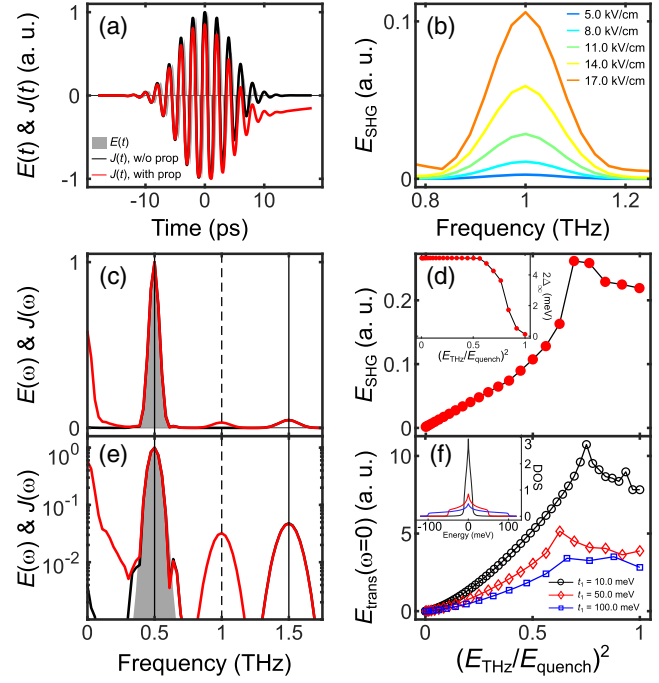

FIG. 4. Gauge-invariant quantum kinetic simulation of dynami-cal symmetry breaking and nonlinear supercurrent photogenera-tion by THz lightwave propagation and interference effects. (a) Dynamics of THz-light-induced nonlinear supercurrent $J(t)$, calculated without (black line) and with propagation effects (red line), together with the representative 0.5 THz pump oscillating electric field used in the calculations (shaded area). (b) Calculated THz SHG for various E-field strengths. (c),(e) Calculated non-linear spectra over a range of frequencies, in linear and semi-logarithmic scale; the linear and THG peaks are indicated by vertical solid lines, while SHG is denoted by vertical dashed line. (d) Calculated nonperturbative THz SHG at 1 THz as a function of the square of the E-field strength normalized by E_{quench} at which the SC order parameter, asymptotically reached, becomes completely quenched (inset). Note there are still SC coherences left at E_{quench} since a part of the Fermi surface remains gapped, different from temperature tuning above T_c in Fig. 3. (f) Fluence dependence of the zero-frequency component of the transmitted nonlinear E field for three different electron hopping strengths t_1 that characterize the flatness of the electronic bands. Inset: DOS for the different t_1 used.

Cooper-pair condensate flow which manifests itself in equilibrium-symmetry-forbidden SHG.

Figure 4(b) presents the calculated SHG spectra of the transmitted electric field for five different electric field strengths. A resonance emerges at the SHG frequency of 1.0 THz with increasing pump fluence in agreement with the experimental observations in Fig. 2(a). The fluence dependence of the SHG signal [Fig. 4(d)] shows a linear dependence as a function of the square of the normalized E field $(E_{\text{THz}}/E_{\text{quench}})^2$ at low electric field strengths, in agreement with the experimental results [Fig. 2(b)]. In this intensity regime the long-time asymptotic order parameter

value Δ_∞ reached after the THz-driven quench is close to the equilibrium value of Δ_{SC} [inset, Fig. 4(d)] such that the dynamics is describable by perturbation expansions. With increasing pump fluence the system enters the nonperturbative regime where the SHG signal shows a nonlinear increase before saturating at elevated pump fields as well as Δ_{SC} becomes significantly quenched by the THz E field [inset, Fig. 4(d)]. Here, the interplay of dynamical symmetry breaking due to $\mathbf{p}_s(t)$ and high harmonic generation (HHG) nonlinearities enhanced by the pairing interaction produce strongly nonlinear quantum dynamics beyond perturbation expansions [13]. Note that the nonperturbative regime can be reached close to E_{THz}, i.e., for field ~ 30 kV/cm at 0.5 THz exceeding the current tabletop THz sources.

To explore the band structure effects on nonlinear supercurrent photogeneration by THz lightwave propagation, we study the effect of the band structure on the photogeneration of the zero-frequency component of the transmitted electric field. For this we use a square lattice nearest-neighbor tight-binding model, $\varepsilon(\mathbf{k}) = -2t_1[\cos(k_x a) + \cos(k_y a)] + \mu$, with nearest-neighbor hopping strength $t_1 > 0$, lattice constant a, and band offset μ. We characterize the effects of the band structure by the DOS close to the Fermi surface. A small electronic hopping parameter t_1 corresponds to flatter band dispersion and large DOS around the Fermi surface; large t_1 yields a small DOS. Figure 4(f) shows the static component of the transmitted electric field $E_{trans}(\omega = 0)$ as a function of normalized electric field strength for three different DOS [inset, Fig. 4(f)] obtained by changing t_1. The photoinduced supercurrent grows with increasing DOS at the Fermi surface, which shows that dynamical inversion symmetry breaking is most effective in SCs with small band dispersion (large DOS) close to the Fermi surface. This is the case for Nb_3Sn SCs here [31,32], in addition to significantly reduced QP scattering compared with, e.g., NbN [13].

In summary, we describe a microscopic mechanism of dynamical symmetry breaking by lightwave acceleration of supercurrent that manifests itself via T-SHG emission forbidden by the equilibrium pairing symmetry. It is absent in normal states partly due to their lack of, e.g., Anderson PS nonlinearities and vanishing current relaxation. Our theory-experiment results reinforce a universal quantum control concept of how oscillating THz electromagnetic field pulses can be used as an alternating-current bias to photogenerate subcycle dynamical spatial symmetry breaking in quantum materials. The light-induced currents and dynamical symmetry tuning can be extended to topological matter with persistent current [16,33,34], 2D materials [35], magnetism [36,37], and unconventional superconductors [38–40].

---

*These authors contributed equally to this work.
†jwang@ameslab.gov
jgwang@iastate.edu

[1] L. Zhao, C. A. Belvin, R. Liang, D. A. Bonn, W. N. Hardy, N. P. Armitage, and D. Hsieh, Nat. Phys. **13**, 250 (2017).

[2] T. Kampfrath, K. Tanaka, and K. A. Nelson, Nat. Photonics **7**, 680 (2013).

[3] X. Yang et al., Phys. Rev. B **99**, 094504 (2019).

[4] R. Matsunaga, N. Tsuji, H. Fujita, A. Sugioka, K. Makise, Y. Uzawa, H. Terai, Z. Wang, H. Aoki, and R. Shimano, Science **345**, 1145 (2014).

[5] T. Cea, C. Castellani, and L. Benfatto, Phys. Rev. B **93**, 180507(R) (2016).

[6] H. Krull, N. Bittner, G. S. Uhrig, D. Manske, and A. P. Schnyder, Nat. Commun. **7**, 11921 (2016).

[7] M. Udina, T. Cea, and L. Benfatto, Phys. Rev. B **100**, 165131 (2019).

[8] A. Kumar and A. F. Kemper, Phys. Rev. B **100**, 174515 (2019).

[9] H. Chu et al., Nat. Commun. **11**, 1793 (2020).

[10] F. Giorgianni, T. Cea, C. Vicario, C. P. Hauri, W. K. Withanage, X. Xi, and L. Benfatto, Nat. Phys. **15**, 341 (2019).

[11] S. Rajasekaran, J. Okamoto, L. Mathey, M. Fechner, V. Thampy, G. D. Gu, and A. Cavalleri, Science **359**, 575 (2018).

[12] X. Yang et al., Nat. Mater. **17**, 586 (2018).

[13] X. Yang, C. Vaswani, C. Sundahl, M. Mootz, L. Luo, J. H. Kang, I. E. Perakis, C. B. Eom, and J. Wang, Nat. Photonics **13**, 707 (2019).

[14] S. Nakamura, Y. Iida, Y. Murotani, R. Matsunaga, H. Terai, and R. Shimano, Phys. Rev. Lett. **122**, 257001 (2019).

[15] T. Cui, X. Yang, C. Vaswani, J. Wang, R. M. Fernandes, and P. P. Orth, Phys. Rev. B **100**, 054504 (2019).

[16] C. Vaswani et al., Phys. Rev. X **10**, 021013 (2020).

[17] Z. Liu et al., Phys. Rev. Lett. **124**, 157401 (2020).

[18] H. A. Hafez et al., Nature (London) **561**, 507 (2018).

[19] See the Supplemental Material at http://link.aps.org/supplemental/10.1103/PhysRevLett.124.207003 for the detailed model and discussions, which includes Refs. [20–24].

[20] F. Yang and M. W. Wu, Phys. Rev. B **100**, 104513 (2019).

[21] F. Jahnke, M. Kira, and S. W. Koch, Z. Phys. B **104**, 559 (1997).

[22] J. Lee, N. Nookala, J. S. Gomez-Diaz, M. Tymchenko, F. Demmerle, G. Boehm, M.-C. Amann, A. Alù, and M. A. Belkin, Adv. Opt. Mater. **4**, 664 (2016).

[23] P. N. Butcher and D. Cotter, in *The Elements of Nonlinear Optics* (Cambridge University Press, Cambridge, England, 1990), pp. 211–245.

[24] A. Mayer and F. Keilmann, Phys. Rev. B **33**, 6954 (1986).

[25] M. J. Stephen, Phys. Rev. **139**, A197 (1965).

[26] T. Yu and M. W. Wu, Phys. Rev. B **96**, 155311 (2017).

[27] Y. Murotani, N. Tsuji, and H. Aoki, Phys. Rev. B **95**, 104503 (2017).

[28] T. Cea, P. Barone, C. Castellani, and L. Benfatto, Phys. Rev. B **97**, 094516 (2018).

[29] H. Haug and A. P. Jauho, *Quantum Kinetics in Transport and Optics of Semiconductors*, Springer Series in Solid-State Sciences (Springer, Berlin, 2007).

[30] V. V. Kozlov, N. N. Rosanov, C. De Angelis, and S. Wabnitz, Phys. Rev. A **84**, 023818 (2011); N. Tsuji and H. Aoki, Phys. Rev. B **92**, 064508 (2015).

[31] B. Sadigh and V. Ozoliņš, Phys. Rev. B **57**, 2793 (1998).

[32] C. Paduani, Solid State Commun. **149**, 1269 (2009).

[33] L. Luo *et al.*, Nat. Commun. **10**, 607 (2019).

[34] X. Yang *et al.*, npj Quantum Mater. **5**, 13 (2020).

[35] See e.g., T. Li, L. Luo, M. Hupalo, J. Zhang, M. C. Tringides, J. Schmalian, and J. Wang, Phys. Rev. Lett. **108**, 167401 (2012).

[36] T. Li, A. Patz, L. Mouchliadis, J. Yan, T. A. Lograsso, I. E. Perakis, and J. Wang, Nature (London) **496**, 69 (2013).

[37] A. Patz, T. Li, X. Liu, J. K. Furdyna, I. E. Perakis, and J. Wang, Phys. Rev. B **91**, 155108 (2015).

[38] X. Yang, L. Luo, M. Mootz, A. Patz, S. L. Bud'ko, P. C. Canfield, I. E. Perakis, and J. Wang, Phys. Rev. Lett. **121**, 267001 (2018).

[39] A. Patz, T. Li, S. Ran, R. M. Fernandes, J. Schmalian, S. L. Bud'ko, P. C. Canfield, I. E. Perakis, and J. Wang, Nat. Commun. **5**, 3229 (2014).

[40] A. Patz, T. Li, L. Luo, X. Yang, S. Bud'ko, P. C. Canfield, I. E. Perakis, and J. Wang, Phys. Rev. B **95**, 165122 (2017).